Journal of the European Ceramic Society **15** (1995) 1047–1059

0955-2219(95)00095-X
0955-2219/95/$9.50

Toughness of Damage Tolerant Continuous Fibre Reinforced Ceramic Matrix Composites

Bent F. Sørensen[a] & Ramesh Talreja[b]

[a]Materials Departrnent, Risø National Laboratory, 4000 Roskilde, Denmark
[b]School of Aerospace Engineering, Georgia Institute of Technology, Atlanta, GA 30332-0150, USA

(Received 30 March 1995; revised version received 24 May 1995; accepted 25 May 1995)

Abstract

A simple shear-lag model is used to estimate the toughness of a unidirectional fibre reinfored ceramic matrix composite. In the model, which includes the residual axial stresses, the stress transfer across the fibre/matrix interface is by a constant shear stress. The estimates from the model are compared to experimental measurements for four composites and good agreement is found. The effects of distributed and localized energy uptake on fracture stability are discussed, and it is concluded that for most applications the toughness, rather than the pull-out energy absorption, should be maximized.

Nomenclature

a	fibre radius
A	cross-section area
B	specimen width
c	crack length
E	Young's modulus
f	fibre volume fraction
G	(critical) energy-release-rate
L	specimen length
l_s	sliding length
l_p	pull-out length
P	applied load
s	spacing of matrix cracks
U	toughness (energy per unit volume) of composite
v	displacement
W_{sl}	energy dissipated (per unit volume) due to frictional sliding
W_p	energy dissipated (per unit area) due to fibre pull out
γ_{WOF}	work of fracture
δ	matrix crack opening
Δ	specimen elongation
ϵ	axial strain
ϵ_u	ultimate tensile strain
Π	potential energy
σ	stress
τ_s	interfacial sliding shear stress
ϕ	strain energy density

Subscript

db	debonding
f	fibre
m	matrix
max	value at specimen separation
mc	matrix cracking
u	value at ultimate stress
FS	full sliding along the interface

Superscript

ACK	fully and multiply cracked matrix
ini	initiation of matrix cracks
res	residual
*	value after specimen separation
0	initial state
I–IV	stages of damage

1 Introduction

Monolithic ceramics are brittle, flaw-sensitive, and of low energy absorption capacity before and during fracture. However, a class of ceramic composites with continuous reinforcement is emerging, which has much more attractive damage and fracture behaviour. Materials in this class are *damage tolerant*, in the sense that the first mode of damage (matrix cracking) does not lead to final fracture. Instead, the strength of the materials is controlled by the strength of the reinforcement. This flaw-insensitive behaviour is a remarkable property of materials that are made of brittle constituents. As a consequence, fracture toughness is not a proper parameter to characterize such materials. Rather, the stress at the onset of multiple matrix cracking, the failure stress, and total energy uptake until failure constitute a set of property parameters.

Most theoretical works on continuous fibre reinforced ceramics focus on two topics: progression of multiple matrix cracking[1–3] and energy dissipation due to fibre pull out.[4–7] Multiple matrix cracking is of importance since it leads to non-linear constitutive behaviour that must be taken into account when these materials are used, see e.g. ref. 8. It is equally important to point out that in general there is no correlation between the 'proportional limit', i.e. the stress level at which multiple matrix cracking causes non-linearity in the stress-strain curve and the fatigue limit.[9] The energy dissipation due to pull out is important for assessment of the final fracture behaviour. A central part of all these models is the role of the interface (see ref. 10 for a recent review).

The energy uptake by distributed mechanisms (i.e. prior to localization) has not been addressed sufficiently in the previous works. Experimentally, a remarkably non-linear stress–strain response has been found for several continuous fibre-reinforced ceramics composites.[9–14] However, the details of the associated evolution of damage have been studied only recently.[15–19] On the basis of these recent findings, this paper develops a model for the energy uptake by distributed mechanisms, defined here as toughness, i.e. the total energy uptake until failure in volume-distributed mechanisms. This energy comprises both the recoverable and non-recoverable parts. It is of major importance, because this is the maximum energy that can be absorbed per unit volume without causing fracture of a component, i.e. (the component will be damaged but will retain its integrity such that it can still continue to carry loads).

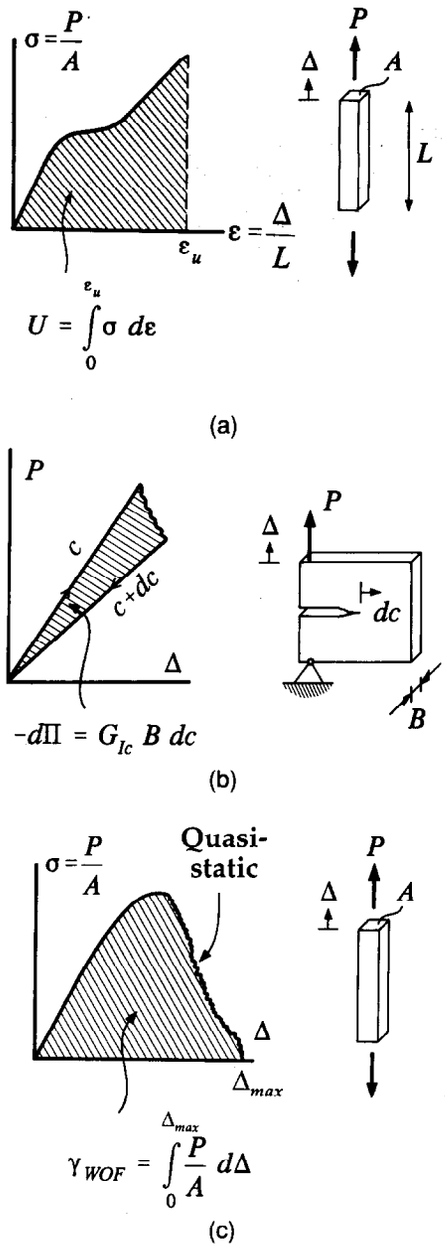

Fig. 1. Energy measures for materials: (A) the toughness, U, (B) the critical energy release rate, G, and (C) the work of fracture, γ_{WOF}.

2 Measurements of energy for material characterization

2.1 Energy quantities

Firstly, for clarity, we start off reviewing some energy concepts and quantities that are often used to characterize the fracture behaviour of materials. For simplicity the considerations are limited to the case where a specimen is loaded by a single tension force. Figure 1 illustrates three commonly used quantities: the toughness, the critical energy release rate (fracture toughness) and the work of fracture.

The toughness[20] is the ability of a material to uptake energy (per unit volume) prior to failure, i.e. the strain energy density to failure[20];

$$U = \int_0^{\epsilon_u} \sigma(\epsilon)\, \mathrm{d}\epsilon, \tag{1}$$

where σ and ϵ are stress and strain, respectively, and ϵ_u is the failure strain (onset of localization). It is the area under the stress–strain curve, and has the SI unit J/m^3.

The *energy release rate* is defined in fracture mechanics by the decrease of the potential energy per new crack area during a quasi-static crack increment[21]

$$G = -\frac{1}{B}\frac{\mathrm{d}\Pi}{\mathrm{d}c}, \tag{2}$$

where Π is the potential energy, and c and B are the length and the width of the crack, respectively. The critical value of G is equivalent to the energy absorbed per unit new crack area, during an incremental (stable) crack growth. The SI unit for G is

J/m^2. Alternatively, the critical value of G is called the fracture toughness. Sometimes in the literature the term toughness is used loosely when fracture toughness is meant. This may cause confusion. In our paper toughness is defined by (1) and fracture toughness by (2).

The *work of fracture* is defined by the total energy absorped (during a quasi-static fracture process) by the specimen per unit fracture area, i.e. the area under the load–displacement curve, per cross-sectional area (see e.g. ref. 22),

$$\gamma_{WOF} = \int_0^{\Delta_{max}} \frac{P(\Delta)}{A} \, d\Delta, \qquad (3)$$

where A is the cross-sectional area of the specimen, P is the load and Δ is the elongation. γ_{WOF} has the SI unit J/m^2.

From the definitions it follows that the quantities mentioned are suited for characterizing different phenomena. U relates the energy uptake (prior to localization) to the volume, and is the proper measure of the *fracture initiation energy*. G is a measure related to characterizing phenomena appearing with *growth of a single crack*. Work of fracture relates the *total energy absorped* (fracture energy) to the full crack area.

2.2 Distributed versus localized energy absorption of uniaxial fibre composites

When unidirectional fibre composites are loaded in the fibre direction a range of *distributed damage* mechanisms occur before final failure. The *fracture* occurs as a *localized* phenomenon, since fibre fracture and pull out only take place at a single matrix crack, namely where the specimen separates into two pieces. Throughout this paper distinction will be made between distributed energy uptake and energy absorped during localization. Distributed energy uptake should be measured by a quantity that reflects that the energy uptake is by distributed phenomena, such as the area under the stress–strain curve, U. The energy dissipation during localization also involves distributed and localized mechanisms. It is of importance to measure and calculate these contributions separately, since they do not scale in the same manner with specimen geometry, as will be elaborated later.

2.3 Choice of test method — bending or pure tension

Having recognised the importance of distinguishing between distributed and localized mechanisms, we now proceed with a discussion of test methods for measurements of the toughness. Materials having distributed damage are characterized by non-linear constitutive laws. Per definition a constitutive law is the relationship between the stress and strain states at any point in the material. For continuum mechanics to be applicable for materials experiencing distributed damage, the test volume (gage length of extensometer or strain gauge) must be much larger than any microstructural dimensions (e.g. matrix crack spacing), such that the measured volume behaviour is scale-independent, and the definitions apply. Moreover, the test *volume* must have *uniform stress and strain fields.*

In bending tests the normal stress distribution is non-uniform (going from tension on one side to compression on the other), and so is the damage evolution, as sketched in Fig. 2. The true stress–strain curve cannot be determined, since the stress and strain distributions across the specimen depth are not known (when damage takes place, the distribution of normal stress is not linear, but depends on the type of damage mechanism and degree of damage). Furthermore, at the peak load, localized fibre failure takes place at the tensile surface, multiple matrix cracking takes place in the central region of the specimen, and the compression side may still be undamaged. From the *bending load–displacement curve it is not possible to distinguish between the effects of distributed mechanisms* (matrix cracking, fibre/matrix debonding and interfacial sliding) and *localized* (fibre breakage and pull out). Furthermore, a shear stress field is present in bending tests. Thus, the damage evolution and failure may be due to shear or compressive stress components, rather than tension.[23]

It is unfortunate that bending tests have been so widely used for characterizing ceramic composites, since this has led to incorrect conclusions concerning the material behaviour. For instance, it has sometimes been suggested that the tail (the downgoing part) of the load–displacement curve (measurable in displacement controlled experiments only) represents the energy dissipation due to fibre

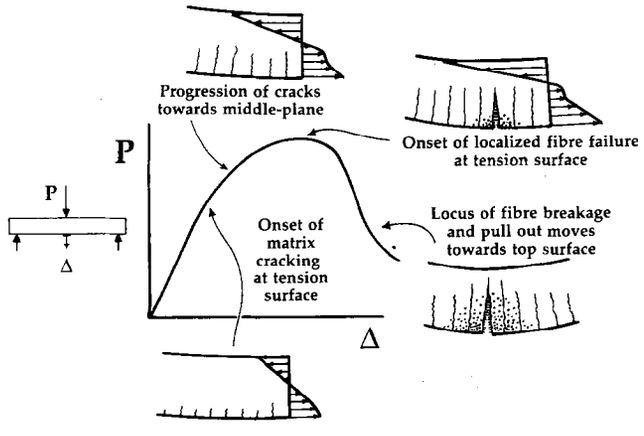

Fig. 2. A schematic illustration of various damage mechanisms operating simultaneously during a bending experiment. The damage evolution is not uniform throughout the depth of the specimen.

pull out. This is incorrect, since matrix cracking, fibre/matrix debonding, fibre sliding and fibre failure continue to take place during this part of the bending response, as the failure locus moves across the depth of the specimen towards the compression side.

Uniaxial tension experiments, on the other hand, allow an unambiguous interpretation, since the damage mechanisms initiate and develop at identifiable stress or strain levels,[15–19] and take place uniformly over the entire volume of the gage section of the specimen.

Unfortunately, tensile tests are difficult to perform, since an accurate alignment is needed to prevent bending effects.[24] Also, although tensile tests are performed with much care, it is not unusual that failure takes place at tabs,[19] so the true strength of the composite cannot always be measured. However, if there is no bending in the test section, then the relationship between stress, strain and damage mechanisms can readily be identified.

2.4 Experimental characterization of damage in uniaxial tension

Figure 3 shows an experimental stress–strain curve of a hot pressed unidirectional SiC-fibre-reinforced calcium alumino silicate (denoted CAS II from Corning Inc., NY, USA) glass–ceramic matrix composite, tested in uniaxial tension along fibres[19] at a strain rate of 4×10^{-4} min^{-1}. Throughout this paper we will refer the evolution of damage to the axial strain of the composite rather than the composite stress, since the axial stress component in the fibres resulting from the external load and the axial stress component in the matrix before matrix cracking are proportional to the axial strain of the composite. This approach also makes it easier to compare behaviour of unidirectional and cross-ply composites. For the SiC/CAS II composite shown in Fig. 3, U was measured to be 3.1 MJ/m^3, which is almost 40 times that of the pure matrix material. However, due to loading rate effects on the monotonic stress–strain behaviour,[25] the value for SiC/CAS II can vary from 1·7 MJ/m^3 (at 0·01 MPa/s) to 5·4 MJ/m^3 (500 MPa/s).

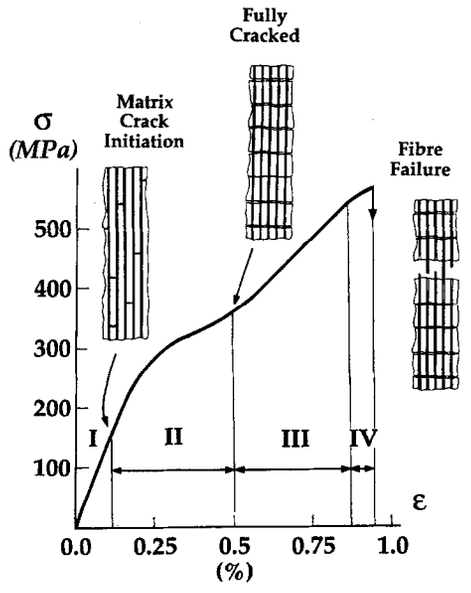

Fig. 3. The non-linear stress–strain curve of SiC/CAS II measured in uniaxial tension along fibres (strain rate of 4×10^{-4}/min). Applied stress as function of strain. The stages of damage evolution are indicated (after ref. 19).

The non-linear stress–strain curve reflects the various stages of damage (see ref. 19 for a detailed discussion). At low strain the material response is linearly elastic and reversible (Stage I). At higher strain matrix cracks initiate and evolve into fairly regularly spaced multiple matrix cracks (Stage II). This takes place over a certain strain range, rather than at a specific strain value. Fibre/matrix debonding also takes place during Stage II, and facilitates frictional sliding along the fibre/matrix interface. These damage processes cause the non-linear part of the stress–strain curve. The corresponding changes in the overall unloading modulus and Poisson's ratio in Stage II can be modelled by a continuum damage model.[8] Increasing the applied stress further leads to a second linear response (Stage III), where the stiffness is mainly due to the fibres. However, significant hysteresis appears during unloading due to effects from interfacial friction. For some specimens a small amount of distributed fibre fracture (Stage IV) may take place just prior to failure. Final failure occurs by localized fibre fracture. Recalling the preceding discussion, the area under the stress–strain curve represents the energy that the material has absorbed per unit volume of the composite up to failure. The energy quantity measured by U is the energy that has been absorbed by *distributed* mechanisms. Mechanisms operating during the *localized* fracture, such as fibre fracture and pull out do *not* contribute to this quantity.

3 Model of Energy Uptake

3.1 Basic considerations

In the following the energy uptake by distributed mechanisms of a unidirectional ceramic fibre reinforced ceramic composite is estimated, based on the damage mechanisms and scenario identified above. The tensile stress–strain curve represents the response of the material to a quasi-static loading in equilibrium with the stresses in the material, and therefore, according to the first law of thermodynamics, the work of the external force must be equal to the change of the energy in the specimen.

In many cases the stress–strain curve does not show non-linearity immediately before failure, indicating that the presence of Stage IV (distributed fibre failure) can be neglected. Thus, our analysis concerns only energy uptake in Stages I, II and III, with Stage III extended until failure. In Stage I the energy uptake per unit volume of the composite, the area under the stress–strain curve up to $\epsilon = \epsilon_{mc}^{ini}$, is denoted U^I. According to the principle of virtual work (or the first law of thermodynamics) the energy uptake U^I is equal to the increase in strain energy density in the matrix and fibres, Φ_m^I and Φ_f^I, respectively, where superscript 0 and I denote the start and end of Stage I, respectively

$$U^I = \int_0^{\epsilon_{mc}^{ini}} \sigma \, d\epsilon = \Phi_m^I + \Phi_f^I - \Phi_m^0 - \Phi_f^0. \quad (4)$$

In Stage II the external work per unit volume is, again, according to the principle of virtual work, equal to the sum of the changes in strain energy density of fibre and matrix, the fracture energy of multiple matrix cracks, fibre/matrix debonding and the energy dissipation due to interfacial frictional sliding in Stage II. Denoting superscript II for the end of Stage II ($\epsilon = \epsilon_{mc}^{ACK}$), the energy uptake in Stage II is

$$U^{II} = \int_{\epsilon_{mc}^{ini}}^{\epsilon_{mc}^{ACK}} \sigma \, d\epsilon = \Phi_m^{II} + \Phi_f^{II} - \Phi_m^I - \Phi_f^I + U_{mc} + U_{db} + W_{sl}^{II}, \quad (5)$$

where W_{sl}^{II} stands for the frictional energy dissipation per unit volume in Stage II, U_{mc} is the energy consumed due to the formation of matrix cracks and U_{db} is the debond energy per unit volume. Assuming that the deformation of fibre and matrix continues in Stage III, the energy uptake in Stage III is

$$U^{III} = \int_{\epsilon_{mc}^{ACK}}^{\epsilon_u} \sigma \, d\epsilon = \Phi_m^{III} + \Phi_f^{III} - \Phi_m^{II} - \Phi_f^{II} + W_{sl}^{III}, \quad (6)$$

where superscript III stands for the end state, when localization sets in ($\epsilon = \epsilon_u$), and W_{sl}^{III} is the frictional energy dissipation in Stage III. This gives the total energy uptake as

$$U = U^I + U^{II} + U^{III} = \Phi_m^{III} + \Phi_f^{III} - \Phi_m^0 - \Phi_f^0 + U_{mc} + U_{db} + W_{sl}, \quad (7)$$

where W_{sl} is the total energy dissipation per unit volume due to frictional sliding in Stages II and III. Note that U can be calculated from the stress and strain states in the *initial and end states*. The frictional energy dissipation can also be calculated from the strain distributions in the end state, assuming the fibre sliding to occur monotonically.

3.2 Basis of unit cell model

In this paper the strain densities and frictional sliding are calculated from a simple shear-lag model, similar to Aveston *et al.*;[1] the effect of residual stresses are added (details are given in the Appendix). The model is a simple one-dimensional analysis, i.e. only the changes in the *axial* stresses and strains are considered, and the interfacial friction shear stress τ_s is assumed to be constant throughout the experiment. This is a good assumption for the accuracy of modelling presented here, since it has been found that the effects of fibre Poisson's contraction and roughness more or less cancel out.[26,27]

Initially, i.e. in the virgin state, the composite is free from external stresses, but has axial residual stresses, σ_f^{res} and σ_m^{res} in the fibre and matrix, due to a thermal expansion mismatch between fibre and matrix. Before fibre/matrix debonding has taken place, there is no slip between fibre and matrix at the interface. During multiple matrix cracking the fibre and matrix debond during the loading, the matrix retracts and, relatively, the fibres slide along the interface monotonically (Fig. 4). It is assumed that the fibres slide symmetrically inside the matrix cylinder from both ends, such that there is sliding along the *entire* interface except at the middle of the matrix cylinder ($0<x<s/2$, Fig. 4), where sticking friction is assumed due to symmetry (the condition for full slip is given in the Appendix).

3.3 Geometrical considerations

A unit cell model is depicted in Fig. 4. The cylindrical volume cell represents a single fibre of radius, a, surrounded by a matrix cylinder. The length of the cell is s, corresponding to the matrix crack spacing, and the outer radius of the matrix cylinder is such that the fibre volume fraction is f. The cross-section area A_f of the fibre is

$$A_f = \pi a^2. \quad (8)$$

The interfacial surface area A_s is

$$A_s = 2\pi a s, \quad (9)$$

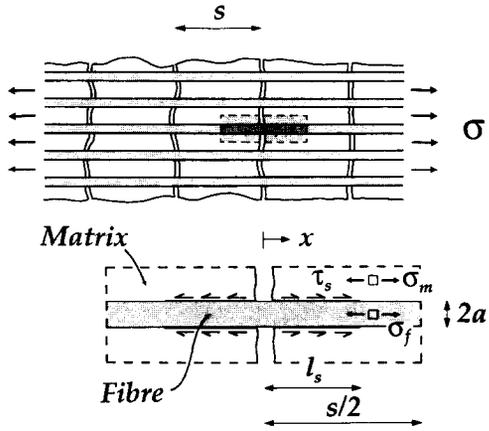

Fig. 4. The axisymmetric unit cell used in the analysis.

the cross-section area of the matrix is

$$A_m = \frac{1-f}{f}\pi a^2 \tag{10}$$

and the total volume of the cell is

$$V = \frac{\pi a^2 s}{f}. \tag{11}$$

3.4 Multiple matrix cracking

During multiple matrix cracking one crack is formed within each volume cell (Fig. 4). Thus the energy absorped per unit volume of the composite is

$$U_{mc} = \frac{G_m A_m}{V} = \frac{G_m}{s}(1-f), \tag{12}$$

where G_m is the critical energy release rate of the matrix, and eqns (10) and (11) have been used.

3.5 Fibre/matrix debonding

For each unit cell there is debonding over the surface A_s, such that the energy absorbed due to fibre/matrix debonding per unit volume of the composite is

$$U_{db} = \frac{G_{db} A_s}{V} = 2f\frac{G_{db}}{a}, \tag{13}$$

where G_{db} is the critical (mode II) energy release rate of the interface, and eqns (9) and (11) have been used. Note that an advantage of this approach is that the estimates of U_{mc} and U_{db} are independent of the load level at which matrix cracking and debonding take place.

3.6 Strain energy in matrix and fibre

The strain energy densities due to residual stresses are

$$\Phi_m^0 = \frac{A_m s}{V}\frac{1}{2}\frac{(\sigma_m^{res})^2}{E_m} = \frac{1-f}{2}\frac{(\sigma_m^{res})^2}{E_m}, \tag{14}$$

and

$$\Phi_f^0 = \frac{A_f s}{V}\frac{1}{2}\frac{(\sigma_f^{res})^2}{E_f} = \frac{(1-f)^2}{2f}\frac{(\sigma_m^{res})^2}{E_f}, \tag{15}$$

where the force balance of the residual stress components in the axial direction,

$$f\sigma_f^{res} + (1-f)\sigma_m^{res} = 0, \tag{16}$$

and eqns 8 and 11 have been used. The strain energy density in the matrix during full sliding along the fibre/matrix interface can be derived from the strain state in the matrix (Appendix), using eqns (10) and (11),

$$\Phi_m^{III} = \frac{A_m}{V/2}\int_0^{s/2}\frac{1}{2}E_m\epsilon_m^2(x)\,dx = \frac{1}{6}\frac{f^2}{1-f}\frac{s^2}{a^2}\frac{\tau_s^2}{E_m}, \tag{17}$$

where the strain is defined to be zero at the stress free state at room temperature. The factor 2 in the denominator before the integral is to account for the integration being only over half the volume of the unit cell shown in Fig. 4 (from the fibre end to the centre of the matrix block).

Likewise, the strain energy density in the fibres during full slip is (by eqns 8 and 11)

$$\Phi_f^{III} = \frac{A_f}{V/2}\int_0^{s/2}\frac{1}{2}E_f\epsilon_f^2(x)\,dx = \frac{1}{2}\frac{\sigma_u^2}{fE_f} + \frac{f}{6}\frac{s^2}{a^2}\frac{\tau_s^2}{E_f} - \frac{1}{2}\frac{\sigma_u}{E_f}\frac{s}{a}\tau_s, \tag{18}$$

where the composite strength is given by the failure strain (Appendix)

$$\sigma_u = f\epsilon_u E_f + \frac{f}{2}\frac{s}{a}\tau_s + f\sigma_f^{res}. \tag{19}$$

3.7 Interfacial frictional sliding

The energy dissipation due to frictional sliding can be assessed by considering the difference in displacement fields between the matrix and fibre at the end state (the maximum applied stress at the point of failure) and the initial state (prestressed with the residual stresses), i.e. from the difference in the displacement fields of fibre and matrix of half the volume cell,

$$W_{sl}(\sigma) = \frac{2}{V}\int_0^{s/2} |\, v_m(\sigma, x) - v_f(\sigma, x)\,|\, 2\pi a\,\tau_s\,dx, \tag{20}$$

where v_m and v_f are the displacement fields of the matrix and fibre at the applied stress σ, defined to be zero before loading (i.e. v_f and v_m are zero when the residual stresses act alone). The factor 2 in front of the integral is to account for the integration being only over the half volume of the unit cell. Using the displacement fields derived in the Appendix, the energy dissipation due to sliding is found by combining eqns (11), (19) and (20),

$$W_{sl} = \frac{f}{2}\frac{s}{a}\left(\epsilon_u + \frac{\sigma_m^{res}}{E_m}\right)\tau_s - \frac{f}{12}\frac{s^2}{a^2}\left(\frac{4f}{1-f}\frac{\tau_s^2}{E_m} + \frac{\tau_s^2}{E_f}\right). \tag{21}$$

Table 1. Properties of fibres, matrices and composites

		SiC/CAS II	*SiC/LAS III*	*SiC/MAS*	SiC/1723
Fibre					
	E_f (GPa)	200	200	200	200
	a (μm)	7·5	7·5	7·5	7·5
Matrix					
	E_m (GPa)	98	85	75[a]	86
	G_m (J/m^2)	25[b]	30[c]	40[a]	40
Composite					
	f	0·35	0·3[d]–0·50	0·45	0·35–0·4
	τ_s (MPa)	5–15[e]	2	1·5[a]	86
	G_{db} (J/m^2)	0·04[f]	0·04[f]	0·04[f]	0·04[f]
	s (μm)	160	400	100	100
	ϵ_u (%)	0·9	0·77[c]	0·36	1·2
	σ_m^{res} (MPa)	70	−50[c]	175	69

The data for SiC/MAS are from ref. 34, [a]supplemented by data for SiC/MAS-L[36].
Data for SiC/CAS II are from ref. 19, except for [b](ref. 17).
The data for SiC/LAS III are from ref. 32; [c]from ref. 33.
[d]Value calculated from the initial composite modulus, E_c.
[e]Lowest value from ref. 31, highest value from ref. 14.
[f]Data from ref. 28.
[g]The data for SiC/1723 are from ref. 12.

4 Results

4.1 Available material data

Table 1 shows the available material data for four continuous fibre-reinforced ceramic composites. The values of G_{db} were taken from Marshall and Oliver,[28] who measured this property on SiC/LAS III with a single fibre push-in method. Since the interphases of most composites consist mainly of carbon,[29,30] an identical value of G_{db} was assigned for all composites. In the literature there is some variation on the values of the interfacial sliding friction for SiC/CAS II, ranging from τ_s = 5 MPa (estimated from the energy dissipation calculated by the fatigue hysteresis loop method[31]) to 15 MPa (found by a single fibre indentation method[14]). For the SiC/LAS III composite[32] Cao *et al.*[33] reported the measured composite modulus E_c to be 120 GPa and a fibre volume fraction of f = 0·5. However, using the rule of mixtures, (eqn 29), f can be calculated from E_c to be f = 0·3. For the SiC/MAS composite[34] a value of $\alpha_m = 5 \times 10^{-6}$ °C^{-1} was used in the calculation of the residual stresses.[35] However, Martin *et al.*[36] reported $\alpha_m = 3 \times 10^{-6}$ °C^{-1} for a MAS-L matrix.

4.2 Comparison of predictions to experiments

Using the material data given in Table 1 and eqns (12)–(15), (17)–(19) and (21), the individual contribution of each mechanism can be calculated, and using eqn (7) the total energy uptake, the value of U can be predicted (Table 2). The experimental results lie close to the theoretical predictions. Some deviations, however, are found, particularly for the SiC/MAS composite. For this material the predicted value is lower than the measured. However, this may be attributed to poor estimates of the residual stresses, since there appears to be some disagreement on the reported values of the thermal expansion mismatch. Neglecting the residual

Table 2. Toughness, predictions and experiments

	SiC/CAS II	*SiC/LAS III*	*SiC/MAS*	*SiC/1723*
U_{mc} (MJ/m^3)	0·10	0·04–0·05	0·22	0·26–0·28
U_{db} (MJ/m^3)	0·004	0·003–0·005	0·005	0·003–0·004
Φ_m^0 (MJ/m^3)	0·016	0·007–0·010	0·11	0·018–0·19
Φ_f^0 (MJ/m^3)	0·015	0·002–0·003	0·05	0·012–0·014
Φ_m^{III} (MJ/m^3)	0·036–0·33	0·003–0·011	0·00–0·007	0·33–0·48
Φ_f^{III} (MJ/m^3)	2·44–2·45	1·90–3·16	0·29	3·95–4·61
W_{sl} (MJ/m^3)	0·17–0·42	0·10–0·16	0·02–0·10	0·84–0·89
U (MJ/m^3)				
Predicted	2·7–3·0	2·0–3·4	0·37–0·46	5·4–6·2
Experiment	3·1	2·7	0·57	5·4

Experimental data for U are from ref. 19 for SiC/CAS II, ref. 33 for SiC/LAS III, ref. 34 for SiC/MAS and from ref. 12 for SiC/1723.

stresses completely gives $U = 0{\cdot}82$ MJ/m^3, which is higher than the experimental value. Thus, it appears that the residual stresses in SiC/MAS, (Table 1), are overestimated. Therefore, it is concluded, that the agreement between prediction and experimental results is satisfactory.

It is interesting that for all the composites the strain energy in the fibres represents more than half of the total energy uptake. Therefore, the most important parameters to raise in order to maximize the toughness are the failure strain and volume fraction of the fibres (see eqns 18 and 19). The contributions from frictional sliding and distributed matrix cracking are significant, whereas the energy absorbed due to debonding is low.

5 Discussion

5.1 Localized energy absorped by fibre pull-out

The energy absorped due to fibre fracture is fG_f per unit cross-section area (assuming, reasonably, that each fibre fails only once during pull-out), where G_f is the critical energy release rate of the fibre. This product is usually very small[6] compared to the energy dissipation due to frictional sliding, and will be neglected in the following. The energy absorption due to fibre pull out can be assessed by the concept of a bridging law (see e.g. ref. 37), where the extra energy absorped due to bridging, ΔG, is given by

$$\Delta G = \int_0^{\delta_{max}} \sigma(\delta)\, d\delta, \tag{22}$$

where δ is the opening of the matrix crack and $\sigma(\delta)$ is the bridging law, i.e. the bridging stress as function of the crack opening. Although eqn 22 was originally derived for bridging in connection with a crack tip,[38] the result is also valid for our problem (in our case the crack can be considered to be infinitely long). For a fibre broken at an average distance l_p away from the matrix crack, the stress in the fibre across the matrix crack (x=0) is (Fig. 5)

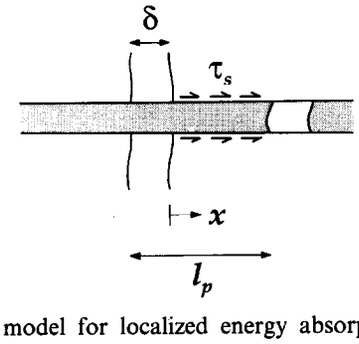

Fig. 5. The model for localized energy absorption by fibre pull-out.

$$\sigma_f(x = 0, \delta) = 2\,\frac{l_p - \delta}{a}\,\tau_s. \tag{23}$$

The bridging stress is $\sigma(\delta) = f\sigma_f(\delta)$, such that the energy absorped due to pull out, W_p, becomes (eqn 22)

$$W_p = \int_0^{l_p} 2_s \frac{l_p - \delta}{a}\,\tau_f\, d\delta = \frac{f l_p^2 \tau_s}{a}, \tag{24}$$

as also obtained elsewhere.[4,7]

Many theoretical efforts have been made to express $\sigma_f(\delta)$ and l_p by the strength variation of the fibres, described by a Weibull distribution, and the interfacial friction.[4–7] This will not be pursued here. Rather, for the purpose of comparing the magnitudes of distributed and localized energies absorped, we simply take the estimates of the mean pull out length by observations from the fracture surfaces. For the SiC/CAS II composite l_p has been reported[17,39] to be in the order of 0·2 mm, giving $W_p = 28$ kJ/m^2.

5.2 Fracture stability and total energy absorption of test specimens

Consider a specimen subjected to uniaxial tension in the fibre direction. Distributed damage (matrix cracking, fibre/matrix debonding and interfacial sliding) operates until the maximum load (the failure load) is reached. From then on the history depends on loading mode. If the test is performed under constant loading rate (load control), the specimen fractures unstably. If the experiment is controlled by the opening of the matrix crack where specimen separation occurs, fracture may take place in a quasi-static manner (solid line, Fig. 6). Although the crack opening, δ, increases monotonically, the overall elongation, Δ, decreases initially, as 'elastic' contraction takes place (due to decreasing load) in the specimen away from the localization. During this unloading the fibres away from the fracture locus contract more in the axial direction than the matrix, leading to energy dissipation by reverse interfacial sliding. In the final stages the overall elongation, Δ, may increase again, if the δ increases with a faster rate than the 'elastic' contraction. In case the experiment is conducted at constant displacement rate, a non-equilibrium load-drop will occur during localization (dashed line, Fig. 6). Depending upon the bridging law and specimen length, L, a tail may occur during separation if the maximum pull out length, $(l_p)_{max}$, is larger than the length change (contraction) due to unloading of the specimen (see Appendix), i.e. if

$$\epsilon_u - \frac{s}{2a}\frac{\tau_s}{E_f} + \frac{\sigma_f^{res}}{E_f} \le \frac{(l_p)_{max}}{L}. \tag{25}$$

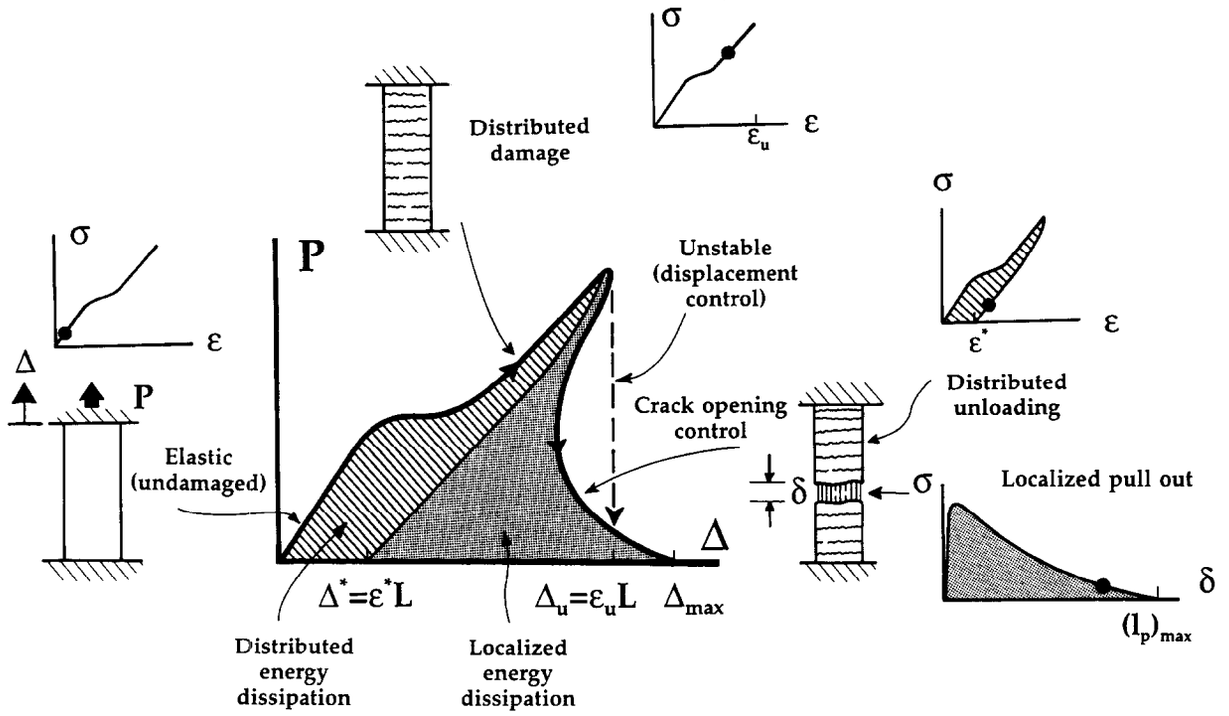

Fig. 6. Schematic illustration of overall load–displacement curve, distributed and localized energy dissipation during loading, fracture and separation of a tensile specimen. The solid line is the load–displacement curve that would occur if the experiment was conducted under crack opening (δ) control, while the dotted line indicates the unstable fracture that takes place under control of the displacement of the specimen. The deformation during loading is due to distributed phenomena, while the down-going part comprises distributed deformation ϵL and localized crack opening δ.

Thus, regarding ϵ_u and $(l_p)_{max}$ as material constants, a tail (stable fracture) will only appear if the specimen length is sufficiently short. Using the material data for SiC/CAS II and SiC/LAS III (Table 1) and $(l_p)_{max}$ = 0·4 mm for the SiC-fibres, the critical length is calculated to be $L \approx 50$ mm. The experimental results of Cao *et al.*[32] were obtained with a gauge length of 15 mm, and a small tail was measured by extensometer. The experiments of Sørensen and Talreja[19] were also conducted in displacement control, but on specimens with longer gage section (80 mm). The fracture occurred unstably (i.e. no tail), although fibre pull out occurred. These results are in agreement with eqn (25). There are examples in the literature where a tail, the down-going part of the load–displacement curve, has been termed as a tough behaviour, contrasting materials that did not show a down-going tail (unstable fracture). Such interpretation is incorrect and should not be accepted. As described above there is no correlation between U and the fracture stability, since *fracture stability is not a material property*, but depends on specimen length and loading condition. Instead, we suggest that attention should be focused on whether amaterial is damage tolerant or flaw sensitive.

As indicated in Fig. 6, the total energy dissipation (the area under the quasi-static load–displacement curve (solid line)) comprises two sources, distributed energy dissipation and localized pull out energy dissipation. During loading the energy dissipation per unit volume by distributed mechanisms is the non-recoverable part of the toughness, i.e. U_{mc}, U_{db}, and W_{sl}. During unloading the reverse sliding that takes place along the fibre/matrix interface dissipates additional energy, W_{sl}^* per unit volume (superscript* indicate unloaded state). When the composite is completely free of external forces, residual stresses exist in fibre and matrix due to interfacial friction, such that strain energy is stored in fibre and matrix. Therefore, the total energy dissipation, from initial undamaged state until the specimen is fully separated, can be calculated as the sum of distributed energy dissipation and localization

$$\int_0^{\Delta_{max}} P(\Delta)\mathrm{d}\Delta = L\,A\,W_D + A\,W_p, \tag{26}$$

where W_D is the energy absorbed per unit volume of the composite by distributed mechanisms,

$$W_D = U_{mc} + U_{db} + W_{sl} + W_{sl}^* + \Phi_m^* + \Phi_f^* - \Phi_m^0 - \Phi_f^0, \tag{27}$$

and W_p is the pull-out energy per unit area. The energy dissipation due to reverse sliding (full slip) per unit volume of the composite is

$$W_{sl}^{*} = \frac{2}{V}\int_{0}^{s/2} | (v_m - v_m^{*}) - (v_f - v_f^{*}) | 2\pi a \tau_s \, dx =$$

$$\frac{s}{2a}\frac{\sigma_u}{E_f}\tau_s - \frac{2}{3}\frac{f}{1-f}\frac{s^2}{a^2}\frac{E_c}{E_m}\frac{\tau_s^2}{E_f}, \quad (28)$$

where E_c is

$$E_c = f E_f + (1-f) E_m. \quad (29)$$

The strain energy of the fibres per unit volume of the composite is (in similar fashion to eqn (18) on noting that the applied stress is zero and the sign in front of τ_s is changed since the slip direction is reversed)

$$\Phi_f^{*} = \frac{f}{6}\frac{s^2}{a^2}\frac{\tau_s^2}{E_f} \quad (30)$$

and that of the matrix is $\Phi_m^{*} = \Phi_m^{III}$. From eqn (26) it follows that the energy dissipation by distributed mechanisms increases with an increasing specimen length, while the pull out energy dissipation does not. An important consequence of this is that the distributed energy dissipation can be raised as much as one desires simply by increasing L. Therefore, the concept of work of fracture, γ_{WOF} (eqn 3), is not applicable for this class of materials.

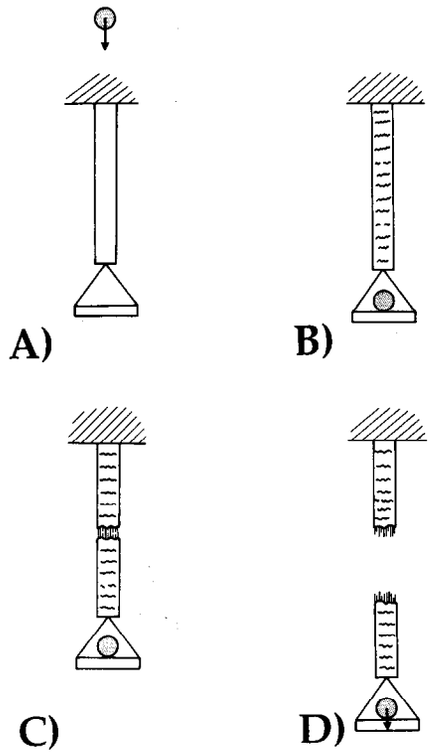

Fig. 7. (A) An impact loading at a component made of a damage tolerant ceramic matrix composite. (B) All the kinetic energy is absorbed by distributed energy uptake. (C) The kinetic energy is absorbed by distributed and localized energy mechanisms. (D) The kinetic energy is higher than what can be absorbed by distributed and localized mechanisms, so the component fractures.

5.3 Energy absorption and fracture stability of components

Now consider an *impact loading of a component* in service (Fig. 7A). This situation is different from a displacement controlled tensile test. In this case it is the actual amount of kinetic energy transferred to the specimen in the form of deformation energy that determines how the fracture behaviour will be. Consider an object hitting the composite component such that the direction of the moving object is in the fibre direction, and that during the impact the object causes uniform tension in the composite. Will the composite break, and in case it does, in which manner?

The first possibility is that the kinetic energy is lower than the total available distributed energy uptake, $U_L A$ (Fig. 7B). Then the composite will absorb the energy without fracture (it will be damaged, but it will not break). Alternatively, when the kinetic energy is higher than $U_L A$, the composite will fracture; the fibres will break, and the composite will lose strength. In this scenario, however, two possibilities exist: (1) If the kinetic energy is higher than the total fracture initiation energy but lower than the total energy dissipation (eqn 26), the component will be damaged and partly fractured (Fig. 7C); with fibres broken and partly pulled out. The composite will lose strength, because the two parts of the composite are only kept together by frictional stresses acting at the broken fibres. (2) If the impact energy is higher than the total fracture initiation energy and higher than the total energy absorped (eqn 26) (Fig. 7D), then the component will fracture unstably, since it cannot absorb the kinetic energy of the object.

Imagine that the component was a turbine blade in a jet-engine (this is a typical considered application for ceramic matrix composites). In such an application it is very important whether or not the component fractures, since a fractured blade may lead to total failure of the engine (this could be fatal for the aircraft). Now, if a turbine blade was hit by a bird or a stone having a specific amount of kinetic energy, what would happen to the component? If $U_L A$ was sufficient to absorb the energy, then the component would be *damaged*, but it would *retain its strength*. Thus, the aircraft would be able to land safely and the damaged component could be replaced. If the impact energy was so high that the component fractured, the pull out energy might stop the object, but now the component strength has decreased. The inertia forces of the rotating component could be sufficiently high that the blade could fracture completely, and the engine would

fail. It follows, that for such applications, the pull-out energy has little importance for the consequences of failure. Therefore, it can be concluded that for such applications it *is not the pull-out energy, W_p, that should be optimized, but the toughness, U.*

6 Conclusions

This paper has analyzed the energy absorption of unidirectional fibre reinforced ceramic composites. A simple model has been used to assess the energy uptake of the individual damage mechanisms. Special attention has been paid to separate energy uptake by distributed and localized mechanisms, since they scale differently with specimen dimensions. The distributed energy uptake, i.e. the toughness, has been found to be mainly due to strain energy in the fibres (this represents more than half of the energy uptake), but contributions from frictional sliding and distributed matrix cracking have also been found to be important, whereas the contribution from fibre/matrix debonding has been found to be very small. The predictions have been compared to experimental values for several composites, and a good agreement between the predictions and the measured values is found. Finally, arguments have been forwarded to conclude that in some applications the energy uptake due to the distributed mechanisms should be maximized rather than the energy for fibre pull-out, giving the most desirable material response.

Acknowledgement

B.F.S. was supported by the Risø Engineering Science Centre for Structural Characterization and Modelling of Materials.

References

1. Aveston, J., Cooper, G. A. & Kelly, A., Single and multiple fracture, *The Properties of Fibre Composites, Conference Proceedings*. IPC Science and Technology Press, Guildford, UK (1971) 15–26.
2. Budiansky, B., Hutchinson, J. W. & Evans, A. G., Matrix fracture in fiber-reinforced ceramics. *J. Mech. Phys. Solids*, **34** (1986) 167–78.
3. McCartney, L. N., New theoretical model of stress transfer between fibre and matrix in a uniaxially fibre-reinforced composite. *Proc. R. Soc. Lond.*, **A425** (1989) 215–44.
4. Sutcu, M., Statistical fibre failure and single crack behaviour in uniaxially reinforced ceramic composites. *J. Mater. Sci.*, **23** (1988) 928–33.
5. Thouless, M. D. & Evans, A. G., Effects of pull-out on the mechanical properties of ceramic-matrix composites. *Acta Metall.*, **36** (1988) 517–22.
6. Curtin, W. A., Theory of mechanical properties of ceramic matrix composites. *J. Am. Ceram. Soc.*, **74** (1991) 2837–45.
7. Cousland, S. McK., The contribution of fibre pull-out to the work of fracture of a metal-matrix composite, for the case of non-interacting fibres. *Materials Forum*, **16** (1993) 327–34.
8. Talreja, R., Continuum modelling of damage in ceramic matrix composites. *Mechanics Materials*, **12** (1991) 165–80.
9. Holmes, J. W. and Sørensen, B. F., Fatigue behavior of continuous fiber reinforced ceramic matrix composites. In *Elevated Temperature Behavior of Ceramic Matrix Composites*, eds S. V. Nair and K. Jakus. Butterworth Heineman, (1995) in press.
10. Evans, A. G., Zok, F. W. & Davis, J., The role of interfaces in fiber-reinforced brittle matrix composites. *Compos. Sci. Technol.*, **42** (1991) 3–24.
11. Prewo, K. M., Fatigue and stress rupture of silicon carbide fiber-reinforced glass-ceramics. *J. Mater. Sci.*, **22** (1987) 2695–701.
12. Mandell, J. F., Grande, D. H. & Dannemann, K. A., High temperature testing of glass/ceramic matrix composites, *Test Methods for Design Allowable for Fibrous Composites*, Vol. 2, ASTM STP 1003, ed. Chamis, C. C. American Society for Testing and Materials (1989) 3–15.
13. Holmes, J. W., Kotil, T. & Foulds, W. T., High temperature fatigue of SiC fibre-reinforced Si_3N_4 ceramic composites. In *Proceedings, Symposium on High Temperature Composites*. Technomic, Basel, (1989) 176–86.
14. Wang, S.-W. & Parvizi-Majidi, A., Mechanical behaviour of Nicalon fiber reinforced calcium aluminosilicate matrix composites. *Ceram. Engng. Sci. Proc.*, **11** (1990) 1607–16.
15. Kim, R. Y. & Pagano, N. J., Crack initiation in unidirection brittle-matrix composites. *J. Am. Ceram. Soc.*, **74** (1991) 1082–90.
16. Barsoum, M. W., Kangutkar, P. & Wang, A. S. D., Matrix crack initiation in ceramic matrix composites, part I. Experiment and test results. *Compos. Sci. Technol.*, **44** (1992) 257–70.
17. Beyerle, D. S., Spearing, S. M., Zok, F. W. & Evans, A. G., Damage and failure in unidirectional ceramic-matrix composites. *J. Am. Ceram. Soc.*, **75** (1992) 2719–25.
18. Karandikar, P. & Chou, T.-W., Characterization and modelling of microcracking and elastic moduli changes in Nicalon/CAS. *Compos. Sci. Technol.*, **46** (1993) 253–63.
19. Sørensen, B. F. & Talreja, R., Analysis of damage in a ceramic matrix composite. *Int. J. Damage Mech.*, **2** (1993) 246–71.
20. Hertzberg, R. W., *Deformation and Fracture of Engineering Materials*, 3rd Edn. John Wiley and Sons, New York, (1989) 26.
21. Kanninen, M. F. & Popelar, C. H., *Advanced Fracture Mechanics*. Oxford University Press, New York, (1985) 159.
22. Sakai, M. & Bradt, R. C., Fracture toughness of brittle materials. *Int. Mater. Rev.*, **38** (1993) 53–78.
23. Marshall, D. B. & Evans, A. G., Failure mechanisms in ceramic-fiber ceramic-matrix composites. *J. Am. Ceram. Soc.*, **68** (1985) 221–31.
24. Holmes, J. W., A technique for tensile fatigue and creep testing of fiber-reinforced ceramics. *J. Compos. Mater.*, **26** (1992) 915–32.
25. Sørensen, B. F. & Holmes, J. W., Effect of loading rate on the monotonic tensile behavior and matrix cracking of a fiber-reinforced ceramic. *J Am. Ceram. Soc.*, (1995) accepted.
26. Marshall, D. B., Shaw, M. C. & Morris, W. L., Measurement of interfacial debonding and sliding resistance in fiber reinforced intermetallics. *Acta Metall. Mater.*, **40** (1992) 443–54.
27. Sørensen, B. F., Effect of fibre roughness on the overall stress–transverse strain response of ceramic composites. *Scrip. Metall. Mater.*, **28** (1993) 435–9.

28. Marshall, D. B. & Oliver, W. C., Measurements of interfacial mechanical properties in fiber-reinforced ceramic composites. *J. Am. Ceram. Soc.*, **70** (1987) 542–8.
29. Bischoff, E., Rühle, M., Sbaizero, O. & Evans A. G., Microstructural studies of the interface zone of a SiC-fiber-reinforced lithium aluminum silicate glass-ceramic. *J. Am. Ceram. Soc.*, **72** (1989) 741–45.
30. Bonney, L. A. & Cooper, R. F., Reaction layer interfaces in SiC-fiber-reinforced glass-ceramics: a high-resolution scanning transmission electron microscopy analysis. *J. Am. Ceram. Soc.*, **73** (1990) 2916–26.
31. Cho, C., Holmes, J. W. & Barber, J. R., Estimation of interfacial shear in ceramic composites from frictional heating measurements. *J. Am. Ceram. Soc.*, **74** (1991) 2808–8.
32. Cao, H. C. & Thouless M. D., Tensile tests of ceramic-matrix composites: Theory and experiments. *J. Am. Ceram. Soc.*, **73** (1990) 2091–4.
33. Cao, H. C., Bischoff, E., Sbaizero, O., Rühle, M., Evans, A. G., Marshall, D. B. & Brennan, J. J., Effect of interfaces on the properties of fiber-reinforced ceramics. *J. Am. Ceram. Soc.*, **73** (1991) 1691–9.
34. Ricca, N., Guette, A., Camus, G. & Jouin, J. M., SiC (ex. PCS)/MAS composite with a BN interphase: microstructure, mechanical properties and oxidation resistance. In *High Temperature Ceramic Matrix Composites, HT-CMC1*, eds R. Naslain, J. Lamon & D. Doumeingts. Woodhead UK (1993) 455–62.
35. Khodakovskaya, R. Y. & Pavlushkin, N. M., Structure and properties of metastable quartzitic phases in sitalls in the SiO_2–Al_2O_3–MgO–TiO_2 system. *Inorg. Mater.*, **3** (1967) 1662–8.
36. Martin, B., Benoit, M. & Rouby, D., Interfacial sliding strength in fibre reinforced ceramic matrix composites mvolving positive radial thermal misfit. *Scripta Metall. Mater.*, **28** (1993) 1429–33.
37. Suo, Z., Bao, G., & Fan, B., Delamination R-curve phenomena due to damage. *J. Mech. Phys. Solids*, **40** (1992) 1–16.
38. Rice, J. R., A path independent integral and the approximate analysis of strain concentrations by notches and cracks. *J. Appl. Mech.*, **35** (1968) 379–86.
39. Rousseau, C. Q., Davidson, D. L. & Campbell, J. B., The micromechanics of ambient temperature cyclic loading fatigue in a composite of CAS glass ceramic reinforced with Nicalon fibers. *J. Comp. Tech. Res.*, **16** (1994) 115–26.
40. Pryce, A. W. & Smith, P. A., Matrix cracking in unidirectional ceramic matrix composites under quasi-static and cyclic loading. *Acta Metall. Mater.*, **41** (1993) 1269–81.

Appendix

A.1 Strain fields

Before matrix cracking and interfacial debonding the composite exhibits residual stresses, e.g. due to thermal expansion mismatch. We define the strains to be zero at stress free state at room temperature. Then the strain fields in matrix and fibres due to the residual stresses are

$$\epsilon_m^{res} = \frac{\sigma_m^{res}}{E_m}, \qquad \text{(A1)}$$

and

$$\epsilon_f^{res} = \frac{\sigma_f^{res}}{E_f}. \qquad \text{(A2)}$$

When matrix cracking and fibre/matrix debonding take place frictional sliding takes place along the interface as the matrix retracts. After application of the external force the strains in the slip region are, with reference to the coordinate system in Fig. 4,

$$\epsilon_m(\sigma, x) = 2\frac{f}{1-f}\frac{x}{a}\frac{\tau_s}{E_m} \quad 0 \le x \le l_s(\sigma) \qquad \text{(A3)}$$

and

$$\epsilon_f(\sigma, x) = \frac{\sigma}{fE_f} - 2\frac{x}{a}\frac{\tau_s}{E_f} \quad 0 \le x \le l_s(\sigma). \qquad \text{(A4)}$$

In these expressions, l_s is the sliding length along the interface, measured from the matrix crack (Fig. 4). The sliding length can be found as the position x along the interface where the fibre and matrix strain changes are identical, $\epsilon_f(l_s) - \epsilon_f^{res} = \epsilon_m(l_s) - \epsilon_m^{res}$, giving

$$\frac{l_s(\sigma)}{a} = \frac{1-f}{2}\left[\frac{\sigma}{f\tau_s}\frac{E_m}{E_c} - \frac{\sigma_f^{res}}{\tau_s}\frac{E_m}{E_c} + \frac{\sigma_m^{res}}{\tau_s}\frac{E_f}{E_c}\right], \qquad \text{(A5)}$$

as also found by Pryce and Smith.[40] From eqns (A5) and (29) it follows that there is sliding along the *entire* interface ($l_s = s/2$), when the applied stress exceeds a characteristic value, σ_{FS} (subscripts indicate Full Slip)

$$\frac{\sigma_{FS}}{fE_f} = \frac{\sigma_f^{res}}{E_f} - \frac{\sigma_m^{res}}{E_m} + \frac{1}{1-f}\frac{s}{a}\frac{\tau_s}{E_f}\frac{E_c}{E_m}. \qquad \text{(A6)}$$

Above this stress level, the stress and strain states in the matrix do not change. This is a consequence of the assumption in the model that τ_s does not change. When the terms of the residual stresses are dropped in eqns (A5) and (A6), they become identical to the results in ref. 31. Inserting the strains gives the strain densities in eqns 17 and 18.

A.2 Displacement fields during loading

The displacement fields at a stress σ (after multiple matrix cracking and debonding) are, for the case of full sliding, then found by integration of the strains,

$$\int_{v_m(x)}^{v_m(x=s/2)} dv_m = \int_x^{s/2}\left[\epsilon_m(\sigma, x) - \frac{\sigma_m^{res}}{E_m}\right]dx \qquad \text{(A7)}$$

and

$$\int_{v_f(\sigma, x)}^{v_f(x=s/2)} dv_f = \int_x^{s/2}\left[\epsilon_f(\sigma, x) - \frac{\sigma_f^{res}}{E_f}\right]dx, \qquad \text{(A8)}$$

where the last terms represent the displacements due to the release of the residual stress during debonding, eqns (A1) and (A2). In eqns (A7) and (A8) $v_m(x=s/2)$ and $v_f(x=s/2)$ are the displacements at the centre of the matrix block. They are identical, since there is no sliding at the centre of the matrix block, and cancel out, when inserting into

eqn (20). Inserting eqns (A3) and (A4) into (A7) and (A8) gives

$$v_m(x) = v_m(x=s/2) - \frac{f}{1-f}\frac{\tau_s}{E_m}\left(\frac{s^2}{4a} - \frac{x^2}{a}\right) + \frac{\sigma_m^{res}}{E_m}\left(\frac{s}{2} - x\right) \quad \text{(A9)}$$

and

$$v_f(\sigma, x) = v_f(x=s/2) + \frac{\tau_s}{E_f}\left(\frac{s^2}{4a} - \frac{x^2}{a}\right) + \left(\frac{\sigma_f^{res}}{E_f} - \frac{\sigma}{fE_f}\right)\left(\frac{s}{2} - x\right). \quad \text{(A10)}$$

Inserting these displacements into eqn 20 gives the frictional energy dissipation (eqn 21).

A.3 Displacement fields during unloading

After fracture, as the specimen unloads the sliding direction changes, as the fibres contract and slide into the matrix. Then, the sign in front of τ_s changes in eqns (A3) and (A4). When the specimen is completely free of external load, the displacement fields are

$$v_m^*(\sigma = 0, x) = v_m^*(x=s/2) + \frac{f}{1-f}\frac{\tau_s}{E_m}\left(\frac{s^2}{4a} - \frac{x^2}{a}\right) + \frac{\sigma_m^{res}}{E_m}\left(\frac{s}{2} - x\right) \quad \text{(A11)}$$

and

$$v_f^*(\sigma = 0, x) = v_f^*(x=s/2) - \frac{\tau_s}{E_f}\left(\frac{s^2}{4a} - \frac{x^2}{a}\right) + \frac{\sigma_f^{res}}{E_f}\left(\frac{s}{2} - x\right). \quad \text{(A12)}$$

Inserting these displacements gives the frictional energy dissipation, W_{sl}^* (eqn 28).

A.4 Overall composite strain

The maximum composite strain during loading can be estimated by the average elongation of the unit cell, using eqn A4 (assuming full sliding),

$$\epsilon_u = \frac{2}{s}\int_0^{s/2} \epsilon_f(\sigma_u, x) - \frac{\sigma_f^{res}}{E_f}\,dx = \frac{\sigma_u}{fE_f} - \frac{s}{2a}\frac{\tau_s}{E_f} - \frac{\sigma_f^{res}}{E_f}. \quad \text{(A13)}$$

The strain offset after unloading is (full sliding)

$$\epsilon^* = \frac{s}{2a}\frac{\tau_s}{E_f} - \frac{\sigma_f^{res}}{E_f}, \quad \text{(A14)}$$

on noting that the sign of in front of τ_s is changed and σ vanishes. Subtracting these two strain values gives the strain change during unloading, i.e. the left hand side of eqn 25.